Journal of Fluids and Structures (2002) **16**(4), 465–485
doi:10.1006/jfls.2001.0433, available online at http://www.idealibrary.com on IDEAL®

APPLICATION OF A MODIFIED k–ε MODEL TO THE PREDICTION OF AERODYNAMIC CHARACTERISTICS OF RECTANGULAR CROSS-SECTION CYLINDERS

K. SHIMADA

Institute of Technology, Shimizu Corporation, 3-4-17 Etchujima, Koto-ku Tokyo 135-8530, Japan

AND

T. ISHIHARA

Department of Civil Engineering, University of Tokyo, 7-3-1 Hongo, Bunkyo-ku Tokyo 113-8656, Japan

(Received 26 October 1998, and in final from 3 September 2001)

Aerodynamic characteristics of rectangular cylinders of infinite length and various breadth-to-depth ratios ranging from $B/D = 0{\cdot}6$ to $8{\cdot}0$ were investigated numerically by a two-layer k–ε model with a modified k-production term. Although the numerical method is two-dimensional (2-D), a physically reasonable smooth, periodic vortex shedding was obtained, even in the range of high Reynolds number. This kind of behaviour cannot normally be simulated by ordinary 2-D analyses which do not incorporate a turbulence model. Various typical aerodynamic features were successfully obtained, particularly including the discontinuity in Strouhal number at the critical section of $B/D = 2{\cdot}8$ and $6{\cdot}0$. Also, drag coefficients and distributions of mean surface pressure were in good agreement with results of experiments and 3-D analyses for the range of B/D ratios. However, as regards the prediction of pressure and force fluctuations, since the currently available Reynolds-Averaged Navier–Stokes models are able to analyse only periodic components and not stochastic components, the total fluctuations in surface pressure and aerodynamic lift force were considerably underestimated in some cases, compared with those measured in experiments and calculated from 3-D analyses.

1. INTRODUCTION

SINCE AN ELONGATED RECTANGULAR CROSS-SECTION is a common configuration found in many structures, such as tall buildings and bridges, it is important in terms of their aerodynamic design to investigate their aerodynamic characteristics in detail.

Bodies with a rectangular cross-section are termed as bluff bodies, in which the separated shear layer generated at the leading edge plays an important role in the production of aerodynamic forces. The behaviour of the shear layer separated from the windward corner and vortices shedding into the wake are dependent on the B/D ratio, where B is the chord length along the direction of flow and D is the depth of the section. Therefore, it is widely recognized that the drag coefficient, lift coefficient and Strouhal number, which defines the periodicity of the shedding vortex, vary with the B/D ratio. Nakaguchi *et al.* (1968) conducted a series of wind-tunnel experiments on bodies with various rectangular

0889–9746/02/040465 + 21 $35.00/0

cross-sections in smooth flow, and demonstrated aerodynamic characteristics specific to rectangular cross-sections, such as the existence of a peak in the drag coefficient near $B/D = 0{\cdot}6$, and a discontinuity of the Strouhal number at $B/D = 2{\cdot}8$. As the aerodynamic behaviour of bodies with rectangular cross-section is characterized by the absence or presence of reattachment of the shear layer, it is divided into three categories: "separated", "intermittently reattached", and "fully reattached", according to the B/D ratio.

Aerodynamic forces acting on a section are generated from the motion of the fluid around the section. Therefore, it is necessary to know the kinematics of the fluid motion around a section to evaluate its aerodynamic characteristics. Numerical procedures presently applied for this purpose are largely classified into two categories: in one, direct numerical simulations are used to solve the Navier–Stokes equation directly, and in the second some type of averaging of the Navier–Stokes equation is performed. In the former case, in particular at large Reynolds number, in general, some type of upwind method for stabilizing the computation is employed to prevent numerical instability caused by the discretization of nonlinear convective terms in the equation. In this category, Tamura & Ito (1996) successfully simulated the aerodynamic characteristics of various rectangular sections in smooth flow by employing the third-order upwind scheme proposed by Kawamura & Kuwahara (1984). The method of averaged Navier–Stokes equation is itself classified into one employing a subgrid scale model and a second known by its acronym as the Reynolds-Averaged Navier–Stokes (RANS) equation model. Murakami & Mochida (1995) successfully reproduced the turbulent statistics of flow around a square cylinder as well as the aerodynamic forces by employing the standard Smagorinsky model. Mochida *et al.* (1996) and Nozawa & Tamura (1998) improved the evaluation of turbulent statistics of a square cylinder by applying a dynamic subgrid scale model in which the Smagorinsky constant, which is kept a constant in the standard Smagorinsky model, was allowed to vary in both space and time. Direct numerical simulation and the method employing the subgrid scale model referred to above are both examples of three-dimensional (3-D) analyses and in both methods it is necessary to use at least 10–20 grid points in the direction perpendicular to the flow. Furthermore, the method employing the third-order upwind scheme which deals with the diffusive effect by the micro-scale turbulent motion with numerical diffusion is in many respects similar to the subgrid scale model. One thing common to all the above methods is that their results are meaningful only when a sufficient spatial resolution is employed; therefore, these methods are memory intensive and require a lot of processing time.

Ohya *et al.* (1992) demonstrated that using a 2-D analysis it was possible to simulate the discontinuity of Strouhal number for $6{\cdot}0 \leqq B/D \leqq 8{\cdot}0$ at $\mathrm{Re} = 10^3$. Nozu & Tamura (1997) pointed out the variation of flow mechanisms around a square cylinder using 3-D computation, showing that 3-D structures begin to appear already as early as $\mathrm{Re} = 2 \times 10^2$, and clusters of small-scale eddies which are a manifestation of three-dimensionality exist in the vortex structure of the wake at $\mathrm{Re} = 10^3$. As their results show, flow around a body of rectangular cross-section is 2-D at relatively low Reynolds number, for which the spanwise momentum transfer seems to be negligible. However, as the Reynolds number becomes higher and exceeds a threshold value, three-dimensionality kicks in and, as a result, remedies are required in numerical procedures to incorporate the physical momentum diffusion in the direction of the span for these procedures to be realistic. The threshold value of the Reynolds number up to which the flow around a body of rectangular cross-section can be considered to be 2-D is of the order of 10^2, and, therefore, results of 2-D computations can only be compared with those from experiments for flows with Re of order of 10^2.

Contrarily, the RANS model enables 2-D computations even in flows with high Reynolds number. This is based upon the hypothesis that, if the spanwise turbulent fluctuation is supposed to be homogeneous, the spatial average of its fluctuation in the direction of the

span is equivalent to its ensemble average. Based on this hypothesis, Franke & Rodi (1991) showed that for a square cylinder in a smooth flow its Strouhal number and mean drag coefficient are reproduced well by the unsteady 2-D analysis using the Reynolds-stress equation model in combination with a wall function. They also showed that if, on the other hand, the conventional standard k–ε model is used in combination with a wall function in an unsteady 2-D analysis, vortex shedding is not simulated, and even with a two-layer model the periodic vortex shedding is weak. As a result a satisfactory agreement could not be obtained with respect to the aerodynamic characteristics. This is because the separation is weakened as excessive amount of turbulent kinetic energy is generated near the frontal corner by the isotropic eddy-viscosity effect (Murakami *et al.* 1990). Kato & Launder (1993) used the property of irrotationality of the flow at the impinging region to remove this defect and proposed a modified k–ε model in which production of turbulent kinetic energy is expressed in terms of a vorticity tensor and a velocity strain tensor. Then they applied this model to a square cylinder and were able to obtain vastly improved predictions of aerodynamic characteristics and turbulence statistics. Later, Kato (1997) using the same model showed that satisfactory results were obtained with respect to the unsteady wind force and vortex-induced vibrations of a square cylinder by using the modified k–ε model combined with a generalized log-law boundary condition, even with a relatively low spatial resolution. Utilizing another scheme, Deng *et al.* (1994) obtained satisfactory results with respect to aerodynamic and turbulence statistics of a square cylinder by using the Baldwin–Lomax model. Similarly, Lee (1997) calculated the flow around a square cylinder by using the standard RNG and the low-Reynolds-number k–ε model in order to evaluate the sensitivity of various parameters associated such as time accuracy, spatial accuracy and choice of convection schemes.

So far, most applications of the RANS model have been confined to square sections. Okajima & Sakai (1991) attempted to apply the standard k–ε model to rectangular cylinders with $B/D = 0{\cdot}6$, $1{\cdot}0$, $2{\cdot}0$ at $\mathrm{Re} = 10^4$; however, further applications to sections with larger B/D ratio have not been tried as yet. They reported that for $B/D = 0{\cdot}6$ and $1{\cdot}0$ a reasonably smooth periodic vortex shedding is simulated and that the drag coefficient and the Strouhal number are close to experimentally obtained values, but for $B/D = 2{\cdot}0$ the Strouhal number is very large and the fluctuating lift coefficient quite small compared with experimentally obtained values. For cross-sections with $2{\cdot}0 < B/D < 2{\cdot}8$, it is known that a double mode exists in the lift fluctuation (Okajima 1983) as a result of an unsteady reattachment of the separated shear layer on the side surfaces. Also, as mentioned above, discontinuities in Strouhal number are evident at $B/D = 2{\cdot}8$ and $6{\cdot}0$. Problems like these pose a tremendous challenge to the development of numerical simulations for modelling flow around rectangular cross-sections. Therefore, it is important to verify its ability to reproduce these phenomena for a further development of the RANS model. In the following section, the modified k–ε model is treated as a RANS model, and its applicability in simulating the aerodynamic characteristics of rectangular cross-sections with $0{\cdot}6 \leqq B/D \leqq 8{\cdot}0$ in smooth flow is investigated.

2. ANALYTICAL METHOD

2.1. Basic Equation

The Reynolds-averaged incompressible Navier–Stokes equation is expressed as follows:

$$\frac{\mathrm{D}U_i}{\mathrm{D}t} = -\frac{\partial}{\partial x_i}\left(P + \frac{2}{3}k\right) + \frac{\partial}{\partial x_j}\left[(\nu + \nu_t)\left(\frac{\partial U_i}{\partial x_j} + \frac{\partial U_j}{\partial x_i}\right)\right], \tag{1}$$

where, v_t is the eddy viscosity coefficient and is given as $v_t = C_\mu k^2/\varepsilon$. The use of averaging operation $\partial\langle\phi\rangle/\partial x_3 = 0$ in the equation, which implies that fluctuation of ϕ in the spanwise direction is homogeneous, and making the substitution $U_3 = 0$ makes equation (1) 2-D. The turbulent kinetic energy k and its dissipation rate ε are obtained by the following transport equations:

$$\frac{\mathrm{D}k}{\mathrm{D}t} = \frac{\partial}{\partial x_j}\left[\left(v + \frac{v_t}{\sigma_k}\right)\frac{\partial k}{\partial x_j}\right] + P_k - \varepsilon, \tag{2}$$

$$\frac{\mathrm{D}\varepsilon}{\mathrm{D}t} = \frac{\partial}{\partial x_j}\left[\left(v + \frac{v_t}{\sigma_\varepsilon}\right)\frac{\partial \varepsilon}{\partial x_j}\right] + (C_{\varepsilon_1}P_k - C_{\varepsilon_2}\varepsilon)\frac{\varepsilon}{k}. \tag{3}$$

The empirical parameters in the equation are given as $C_\mu = 0{\cdot}09$, $C_{\varepsilon_1} = 1{\cdot}44$, $C_{\varepsilon_2} = 1{\cdot}92$, $\sigma_k = 1{\cdot}0$ and $\sigma_\varepsilon = 1{\cdot}3$, all of which are identical to those used in the conventional, standard k–ε model. Since in the case of the standard k–ε model these empirical constants are identified from temporal means of experimentally measured values, justification of their application to the present model in the sense of ensemble averaging is questionable. However, as judged from the results which are discussed in Section 3, any uncertainties arising from these model constants were not observed.

In equation (3), P_k is the production term of turbulent kinetic energy. In the standard k–ε model, this is given by

$$P_k = C_\mu \frac{k^2}{\varepsilon}\frac{1}{2}\left(\frac{\partial U_i}{\partial x_j} + \frac{\partial U_j}{\partial x_i}\right)^2. \tag{4}$$

However, when using this formula, it is widely recognized that excessive amounts of turbulent kinetic energy are produced near the leading edges of the cross-section. In the present analysis, a model proposed by Kato & Launder (1993) in which the production term is modified based on the assumption of flow irrotationality is employed:

$$P_k = C_\mu \frac{k^2}{\varepsilon}\sqrt{\frac{1}{2}\left(\frac{\partial U_i}{\partial x_j} + \frac{\partial U_j}{\partial x_i}\right)^2}\sqrt{\frac{1}{2}\left(\frac{\partial U_i}{\partial x_j} - \frac{\partial U_j}{\partial x_i}\right)^2}. \tag{5}$$

2.2. Turbulence Model Near Solid Boundary

Proper treatment of boundary conditions is important for a simulation of flow field around rectangular cross-sections, as the flow is involved with separation and reattachment as it passes through the bodies. Previous works on the k–ε model have used the generalized log-law near a solid boundary without employing a sufficient number of grid points for reasons of economy. However, for flow around a rectangular cross-section in which separation and reattachment are involved, the validity of the generalized log-law is questionable. Furthermore, if the log-law is used, the effect of the Reynolds number on these phenomena is not precisely reflected. Therefore, the present scheme employs the low-Reynolds-number one-equation model which is henceforth referred to as the two-layer model (Norris & Reynolds 1975; Rodi 1991). That is, the k equation is solved by assigning $k = 0$ on the solid boundary. Instead of solving the ε equation, ε near the wall is determined by the turbulent kinetic energy k using a length scale l_ε. The eddy viscosity v_t in the region in which the ε equation is not solved is calculated using the turbulent kinetic energy k and a length scale l_μ same as ε,

$$\varepsilon = \frac{k^{3/2}}{l_\varepsilon}, \qquad v_t = C_\mu k^{1/2} l_\mu. \tag{6}$$

The length scales l_ε and l_μ are proportional to turbulent eddy scale l ($= \kappa y$) and are determined using the following relations:

$$l_\mu = C_l y\left[1 - \exp\left(-\frac{\mathrm{Re}_y}{A_\mu}\frac{25}{A^+}\right)\right], \qquad l_\varepsilon = \frac{C_l y}{1 + 5{\cdot}3/\mathrm{Re}_y}, \tag{7}$$

where the constants are given as $C_l = \kappa C_\mu^{-3/4}$, $A_\mu = 50{\cdot}5$ and $A^+ = 25$. In the two-layer model since l_ε and l_μ are functions of the turbulent Reynolds number Re_y ($= k^{1/2}y/\nu$), the effects of the Reynolds number on flow around bodies with rectangular cross-sections can be evaluated. The Reynolds number is known to be important for describing the aerodynamic characteristics of bodies with a curved surface such as a circular cylinder. Numerical studies using the two-layer model conducted by Shimada & Meng (1997) were successful in simulating the variation of the drag coefficient of a circular cylinder with the Reynolds number.

In the present calculation, the two-layer model is applied to the region only within three meshes away from the solid boundary. Also, in order to evaluate the aerodynamic forces as accurately as possible, the flow structure must be finely resolved in the immediate vicinity of the regions on the cross-section where steep gradients exist in the physical quantities and the behavior of the separated shear layer needs to be captured as correctly as possible. To achieve this, a generalized curvilinear coordinate system (body-fitted coordinate system) is incorporated to be able to concentrate a sufficient number of grid points near the boundary.

2.3. Time-Marching, Convective Term and Pressure

The foregoing set of equations is transformed by using a generalized coordinate system and is then solved by the finite difference method. The time-marching algorithm follows the Marker and Cell method by Harlow & Welch (1965). In the method, the conservation of mass is incorporated by solving the Poisson equation for pressure, and subsequently the momentum transport equations are solved for the respective velocity components using the updated pressure. The convective term in the velocity transport equation is discretized by a third-order upwind difference scheme proposed by Kawamura & Kuwahara (1984), and the convective terms in the k and ε transport equations are discretized by a first-order upwind difference scheme, to stabilize the numerical instability at high Reynolds number arising from the nonlinear effect of the convective term. Time is advanced using a first-order Euler implicit scheme. In particular, when one considers the simulation to extend to the realm of aeroelastic vibrations, it is necessary to advance the time from about some hundreds to a thousand of the reduced time, and therefore time advancement in an explicit manner is not a reasonable choice. Keeping these points in mind, in the present calculation it was decided to proceed with the calculation in a stable manner, so as to be able to simulate vortices which are as large as the Karman vortex rather than to attempt to precisely reproduce the turbulence statistics.

The pressure is obtained by solving the Poisson equation for pressure which is obtained by applying the divergence operator on the momentum transport equation and is given as

$$\nabla^2 P = -\frac{\partial}{\partial x_i}\left(U_j\frac{\partial U_i}{\partial x_j}\right) + \frac{\partial^2}{\partial x_i \partial x_j}\left[\nu_t\left(\frac{\partial U_i}{\partial x_j} + \frac{\partial U_j}{\partial x_i}\right)\right] + \frac{\nabla_i U_i^n}{\Delta t}. \tag{8}$$

The second term on the right-hand side of equation (8) comes from the Reynolds stress term, and this is produced from convective term as recognized from the definition; hence this term was kept in the source term.

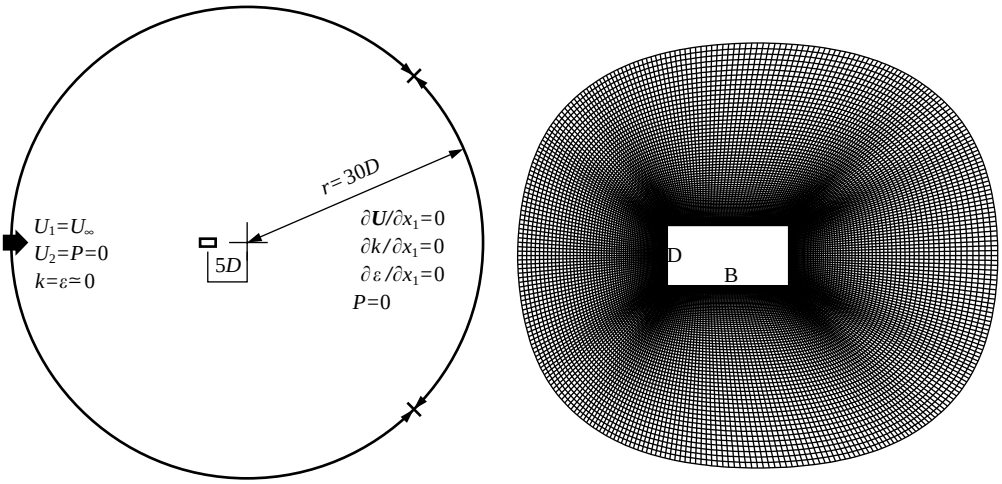

(a) (b)

Figure 1. (a) Analytical domain and boundary conditions, and (b) grid system near the section.

TABLE 1
Spatial resolution

B/D	Grid points
0·6, 1·0	200×200
$1{\cdot}0 < B/D \leq 8{\cdot}0$	320×200

2.4. Grid System and Boundary Condition

The analytical domain is a circle with a radius of $30D$, and the body with a rectangular cross-section is placed at a distance of $5D$ upstream from the center of the domain as shown in Figure 1. The number of grid points used in the runs of calculation are summarized in Table 1.

Figure 1 also shows the boundary conditions. At the inlet boundary, smooth flow with $U_1 = U_\infty$ is imposed as the boundary condition. The turbulent kinetic energy and its dissipation rate are $k = 10^{-5}\ \mathrm{m}^2/\mathrm{s}^2$ and $\varepsilon = 10^{-5}\ \mathrm{m}^2/\mathrm{s}^3$, respectively. At the outlet boundary, a Neumann-type boundary condition with $\partial \mathbf{U}/\partial x_1 = 0$ is imposed. Pressure on the perimeter of the domain is set to zero, and on the solid boundary its normal derivative is set to zero.

The Reynolds number is chosen to be $\mathrm{Re} = U_\infty D/\nu = 2{\cdot}2 \times 10^4$, so as to be consistent with the experiment by Lyn (1992), in which turbulent statistics around a square prism were measured in detail. Almost all other experiments referenced in the following discussion are carried out at a Reynolds number of the order of 10^4.

3. RESULTS AND DISCUSSION

3.1. Verification of the Numerical Method ($B/D = 1{\cdot}0$)

At first, the aerodynamics of a rectangular body with $B/D = 1{\cdot}0$, which was investigated in detail experimentally and numerically, is discussed for the purposes of validating the general

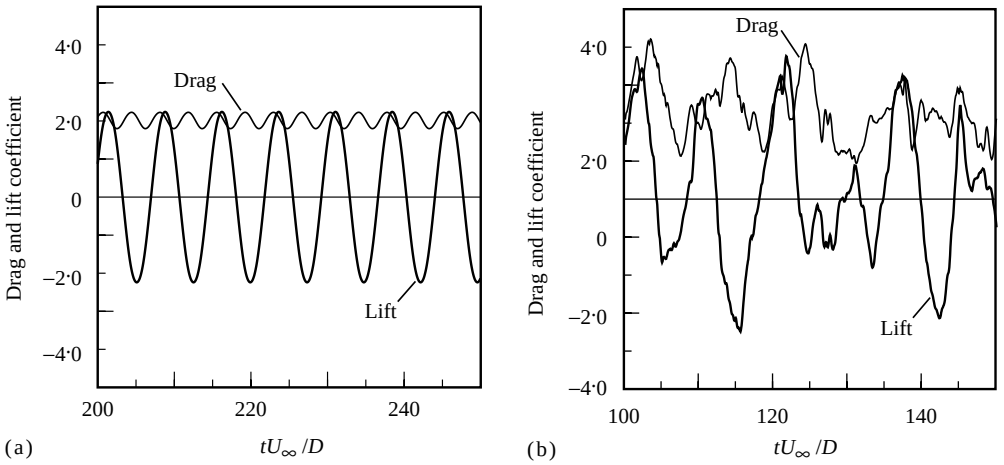

Figure 2. Time histories of drag and lift coefficients for a $B/D = 1{\cdot}0$ rectangular cross-section (200×100): (a) Case 1 (present calculation); (b) Case 2 (2-D calculation without the turbulence model).

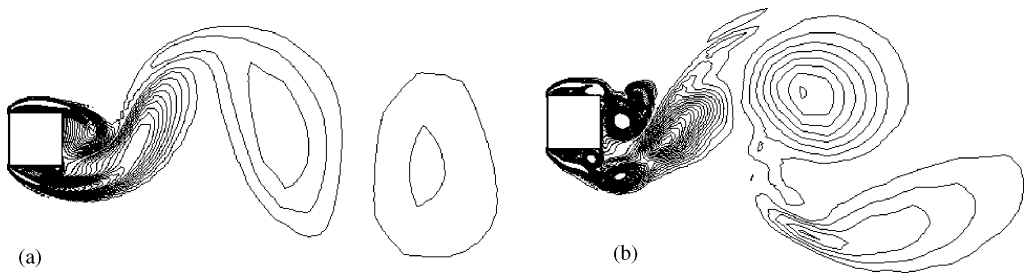

Figure 3. Instantaneous vorticity contours around a $B/D = 1{\cdot}0$ rectangular cross-section (200×100): (a) Case 1 (present calculation); (b) Case 2 (2-D calculation without the turbulence model).

applicability of the 2-D approach using the RANS model and verifying the present numerical code. In Figure 2, time histories of aerodynamic force coefficients obtained by the present numerical calculation are illustrated as Case 1 and those from an ordinary 2-D analysis, in which simply $u_3 = 0$ is imposed, where $u_3 = \bar{U}_3 + u'_3$ are presented as Case 2. Case 1 records show an almost sinusoidal periodic fluctuation; however, in Case 2 the fluctuations are random and their amplitudes are quite large.

Figure 3 compares the instantaneous vorticity as calculated by these two methods. In Case 1, an apparent Karman vortex street is formed in the wake of the cross-section, while in Case 2 the shed vortices downstream of the cross-section do not advect directly. When an approach similar to that used in Case 2 is employed, this kind of defective phenomenon is always observed in the range of Reynolds number over 10^4. This is supposed to arise from the fact that the momentum, which should otherwise be diffused in the spanwise direction by 3-D turbulent mixing, is unable to diffuse properly when an ordinary 2-D procedure which leads to a concentration of extremely strong vorticity like those found in Figure 3(b) is used. On the other hand, Case 1 incorporates the turbulent diffusive effect adequately and even at high Reynolds numbers is successful in simulating smooth periodic vortex shedding by avoiding an excessive concentration of vorticity.

In Table 2, aerodynamic force coefficients obtained by the present numerical simulation are compared with some previously obtained numerical results and with the results of an

TABLE 2
Comparison of aerodynamic properties

	C_D	C'_D	C'_L	St
Franke & Rodi (1991) (RSE + w.f.)	2·15	0·383	2·11	0·136
Kato & Launder (1993) (MP k–ε + w.f.)	2·05 ± 0·03		1·16	0·145
Present calculations (200 × 200)	2·05	0·093	1·43	0·141
Sakamoto *et al.* (1989) (Experiment)	2·22	0·132	1·45	0·134

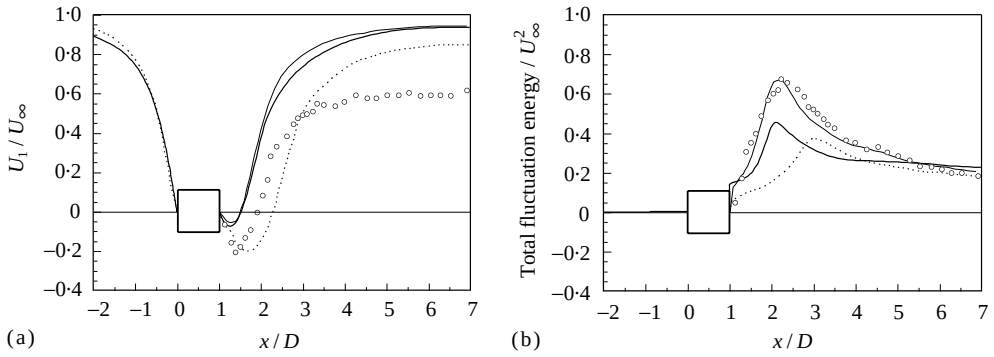

Figure 4. Distribution of time mean turbulence statistics on the centre-line in the flow of $B/D = 1{\cdot}0$ rectangular cylinder: (a) U_1-component; (b) total fluctuation (periodic component + stochastic component). —, Present calculation (200 × 100); —, Franke & Rodi (1991) (RSE + w.f.); - - -, Kato & Launder (1993) (MP k–ε + w.f.); ○, experiment by Lyn (1992).

experiment conducted by Sakamoto *et al.* (1989). With respect to the mean drag coefficient, the results from all the RANS models are in reasonably good agreement with the experimental result, although they are all slightly below the experimental value. However, there are some differences in the fluctuating lift coefficient. Arranged in decreasing order of magnitude, the fluctuating lift coefficients line up like this: [Franke & Rodi] > [our calculation] > [Kato & Launder]. In order to account for this difference, the distribution of the mean velocity and of the total fluctuating energy, consisting of both periodic and stochastic components, along the centre-line in the wake field is presented in Figure 4.

The size of the reversed flow region formed behind the prism which is described as a region in which $U_1/U_\infty < 0$ as evaluated by our calculation and by Franke & Rodi is seen to be excessively narrow compared to the experimentally obtained reversed flow region, as shown in Figure 4(a), but that by Kato & Launder is larger. The differences in the estimated size of the reversed flow region can be associated with the differences in magnitude of turbulent mixing in the wake of the prism, which is illustrated as the total fluctuating energy in Figure 4(b). Franke & Rodi report the largest total fluctuating energy and the highest fluctuation in lift, and on the other extreme Kato & Launder report the lowest total fluctuating energy and the lowest fluctuation in lift. This means that the fluctuation in lift can be related to the turbulent mixing in the wake of the prism and the size of the wake. These observed differences might arise from the differences in the treatment of the turbulence model near the solid boundary and/or the convection scheme. Kato *et al.* suggested that treatment of the flow near the solid boundary significantly affects the turbulence statistics and, also, the aerodynamic characteristics.

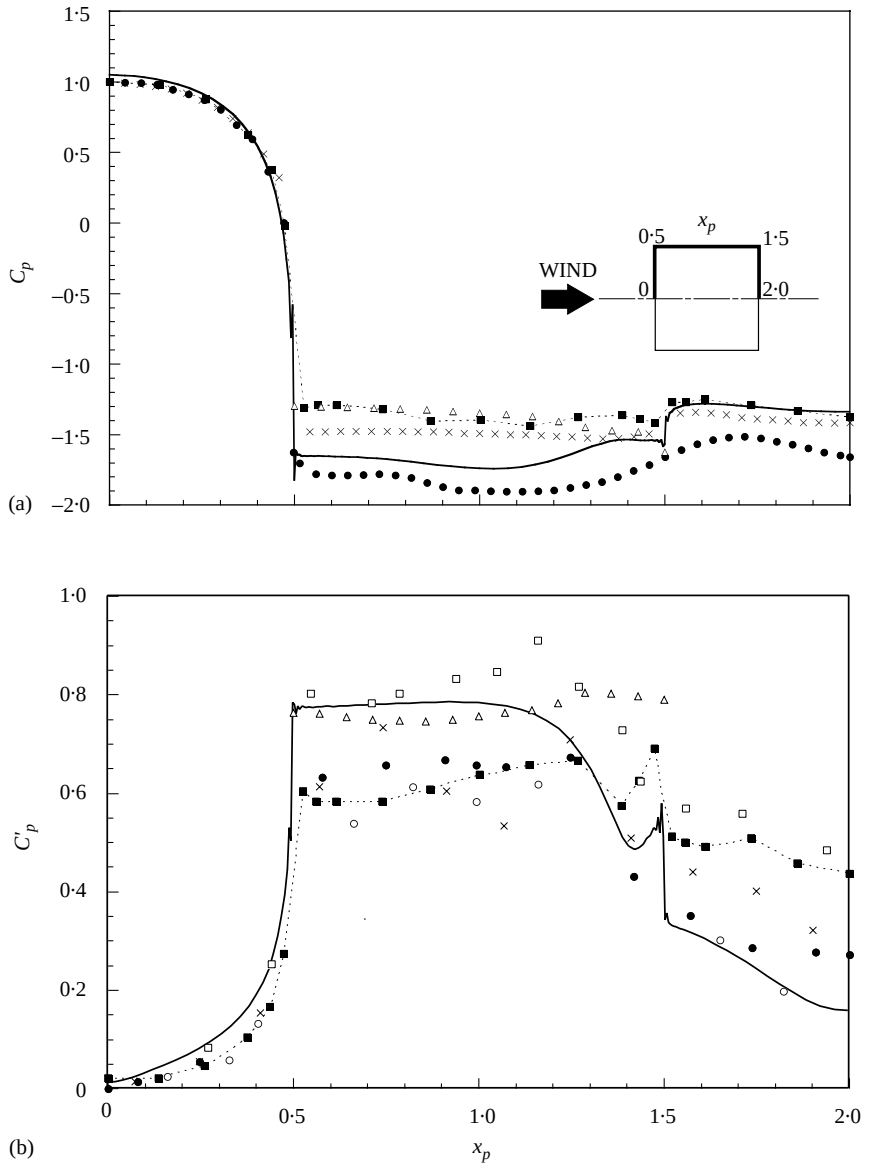

Figure 5. Pressure distribution of $B/D = 1{\cdot}0$ rectangular section: (a) mean pressure distribution; (b) fluctuating pressure distribution. ■, Otsuki *et al.* (1978), $\mathrm{Re} = 0{\cdot}65\text{–}0{\cdot}76 \times 10^5$, $I = 0{\cdot}2\%$, $\gamma_b = 5{\cdot}4\%$, $H/D = 6{\cdot}25$; ●, Bearman & Obasaju (1982), $\mathrm{Re} = 0{\cdot}2 \times 10^5$, $I = 0{\cdot}18\%$, $\gamma_b = 5{\cdot}5\%$, $H/D = 17$; □, Pocha (1971), $\mathrm{Re} = 0{\cdot}92 \times 10^5$; ×, Lee (1975), $\mathrm{Re} = 1{\cdot}76 \times 10^5$; ○, Wilkinson (1974), $\mathrm{Re} = 0{\cdot}1\text{–}1{\cdot}0 \times 10^5$; where I is the turbulence intensity, γ_b the blockage ratio, and H/D the aspect ratio of the model. —, Present calculations; △, Tamura & Ito (1996) 3-D calculations.

Figure 5 shows the distributions of mean and fluctuating pressure coefficients. Rectangular cross-sections with $B/D = 1{\cdot}0$ are classified as separated-type cross-sections. This is because their side-surfaces are completely immersed in the separated flow region with the shear layer which becomes separated at the leading edge of the cross-section and it does not make an apparent reattachment to the side surfaces. Therefore, on the side-surfaces there is suction pressure, and its distribution does not exhibit large variations. In Figure 5, although

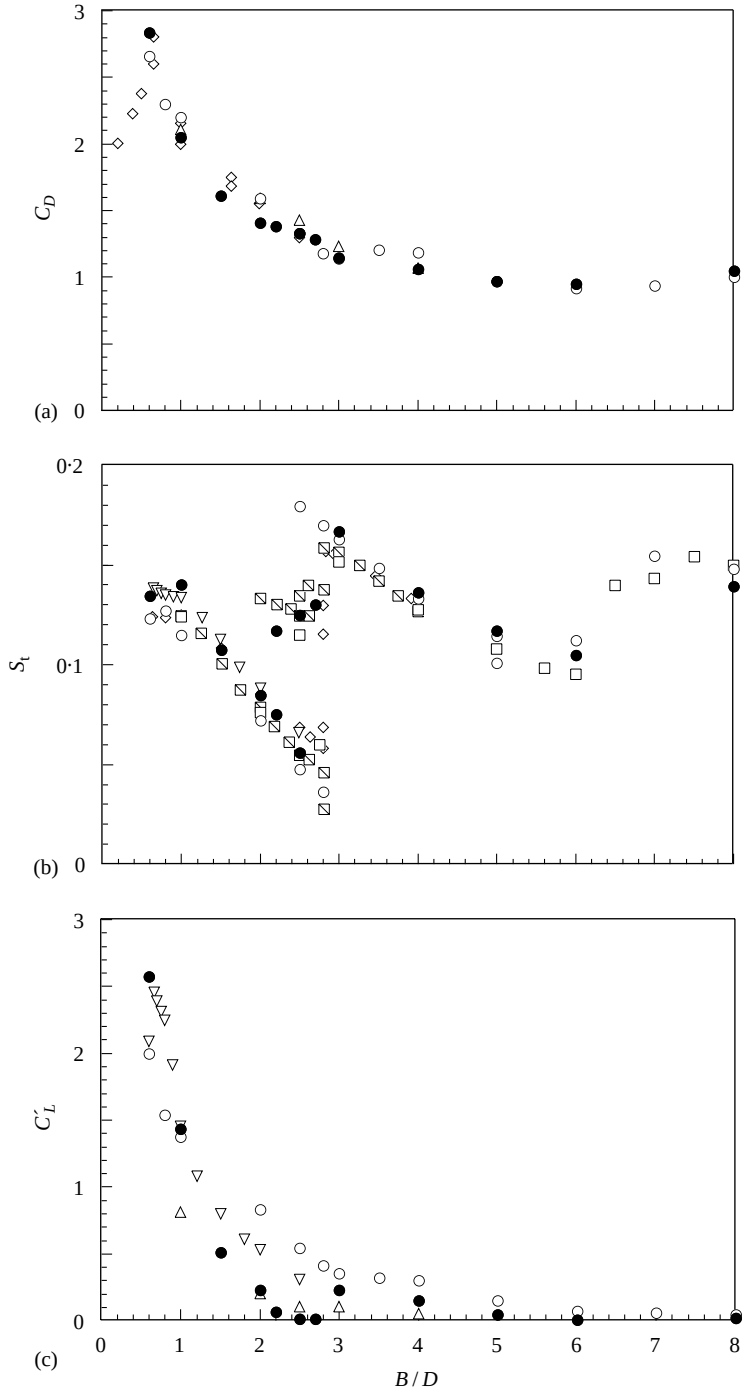

Figure 6. Variations of aerodynamic characteristics according to B/D ratio: (a) mean drag coefficient; (b) Strouhal number; (c) fluctuating lift coefficient. ◇, Nakaguchi *et al.* (1968) $\mathrm{Re} = 0{\cdot}2\text{–}0{\cdot}6 \times 10^5$, $\gamma_b = 2{\cdot}8\%$, $H/D = 14$; △, Otsuki *et al.* (1978), $\mathrm{Re} = 0{\cdot}65\text{–}0{\cdot}76 \times 10^5$, $I = 0{\cdot}2\%$, $\gamma_b = 5{\cdot}4\%$, $H/D = 6{\cdot}25$; □, Okajima (1983), $\mathrm{Re} = 0{\cdot}42 \times 10^5$, $\gamma_b = 1\%$, $I = 0{\cdot}4\%$; ▽, Sakamoto *et al.* (1989), $\mathrm{Re} = 0{\cdot}55 \times 10^5$, $\gamma_b = 7\%$, $H/D = 9{\cdot}5$; where I is the turbulence intensity, γ_b the blockage ratio, and H/D the aspect ratio of the model. ○, Tamura & Ito (1996) 3-D calculations; ●, present calculations.

the experimental values are seen to exhibit some amount of scattering in both the mean and the fluctuation coefficients, the present result almost coincides with the experimental results.

Thus, for stationary cross-sections, the modified k–ε model which is incorporated in the present analysis is seen to lead to a satisfactory result with respect to prediction of the aerodynamic characteristics, although it provides a rather poor estimation of the turbulence statistics of the flow.

3.2. Variation of Aerodynamic Characteristics with B/D Ratio

Figure 6 shows the effect of varying the B/D ratio on (a) the mean drag coefficient, (b) the Strouhal number $\mathrm{St} = nD/U_\infty$ which is obtained from the peaks in the spectrum of the lift, where n is a dominant frequency in the spectrum, and (c) the fluctuating lift coefficient, in which, in the calculation, only the periodic component is considered. In the figure, wind-tunnel experimental results (Nakaguchi *et al.* 1968; Okajima 1983; Otsuki *et al.* 1978; Washizu *et al.* 1978; Sakamoto *et al.* 1989) and results of a 3-D numerical simulation (Tamura & Ito 1996) are presented for the sake of comparison. General features common to the measurements and analytical results are as follows.

The mean drag coefficient shows a peak near $B/D = 0{\cdot}6$ and decreases monotonically as the B/D ratio increases. The Strouhal number exhibits discontinuities at $B/D = 2{\cdot}8$ and near $B/D = 6{\cdot}0$. The number of available data on the fluctuating lift coefficient is not enough for a comparison, but it does show a tendency to decrease monotonically, starting at $B/D = 0{\cdot}6$. The results of our numerical simulation are almost consistent with both the experimental results and those of 3-D numerical analyses, in particular with respect to the mean drag coefficient and the Strouhal number. As for the fluctuating lift coefficient, our numerical results are relatively small in value compared to those of the experiment and 3-D analyses. This point will be discussed in more detail later in Section 3.3.

Instantaneous vorticity contours are illustrated in Figure 7 to graphically show the flow pattern around the cross-sections in an attempt to understand the aerodynamic characteristics mentioned above. In general, the results of an unsteady 3-D analysis show small-scale eddy structures due to the 3-D turbulent motion in the vicinity of the boundaries of the cross-sections. However, no such small-scale eddies are visible in the output of the present analysis which uses the RANS model. This is because a perturbation such as small-scale eddies from the ensemble averaged fluctuation is regarded as turbulence numerically, which is incorporated as eddy viscosity in the equation; hence such small-scale eddies are obscured by the turbulent viscosity effect.

When the flow regime on the side-surface of the cylinder, such as reattachment of the separated shear layer, is observed, it is useful to visualize it by streak lines rather than by vorticity. Figure 8 shows the streak lines of cross-sections with typical B/D ratios of 2·0, 3·0 and 8·0, where the vortex-shedding period is the largest for $B/D = 2{\cdot}0$, the Strouhal number is the largest for $B/D = 3{\cdot}0$, and a steady reattachment is observed for $B/D = 8{\cdot}0$. Figure 9 depicts the mean and fluctuating surface pressure distributions on the side surface for a range of B/D ratios.

3.2.1. *Separated-type cross-sections* ($B/D < 2{\cdot}8$)

In the separated-type rectangular cross-sections, a periodic and apparent vortex shedding can be observed, as illustrated in Figure 7(a–e). Examining the mean pressure coefficient, it is seen in Figure 9(a) that for $B/D = 1{\cdot}0$ and 2·0, although there is pressure recovery on the side-surfaces, the pressure recovery is approximately 10% of the largest suction, and it is small compared with that of other cross-sections which range between 70 and 90%.

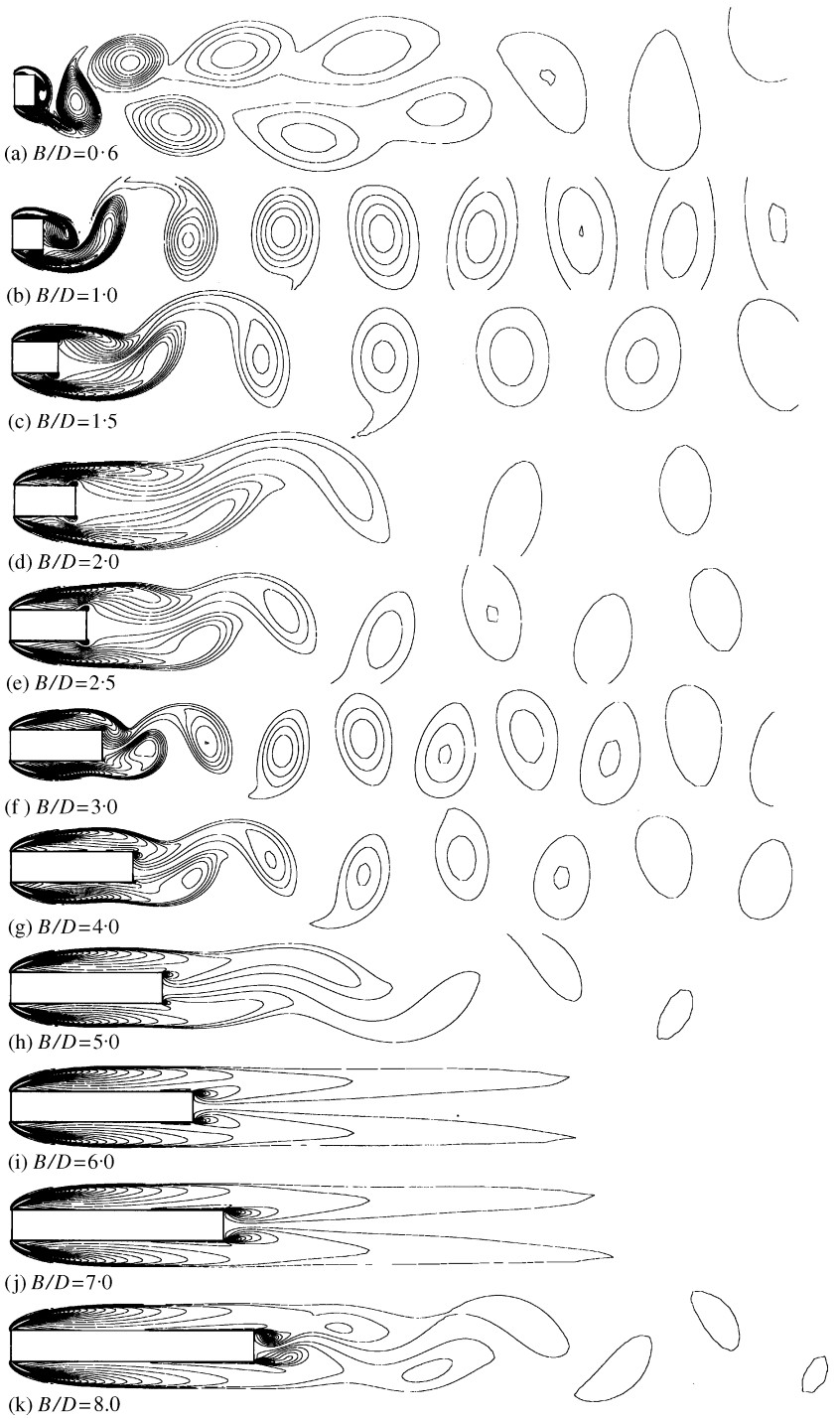

Figure 7. Instantaneous vorticity contours around rectangular cross-sections with various B/D ratios at the maximum lift.

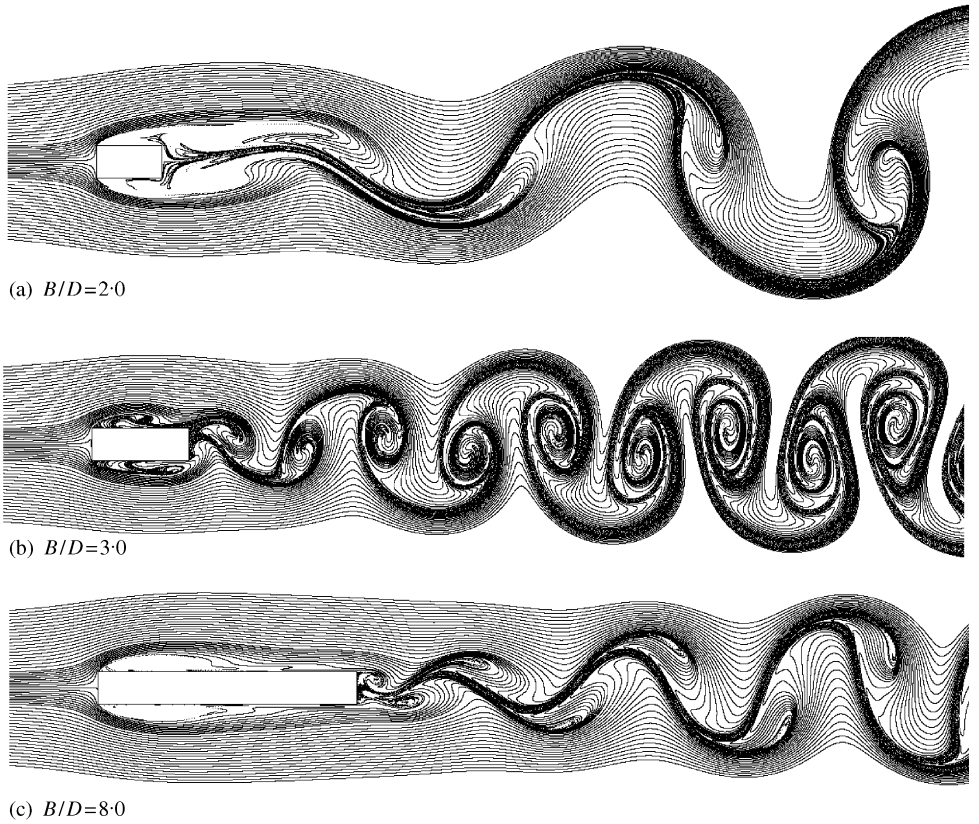

Figure 8. Streak lines obtained by the present calculation.

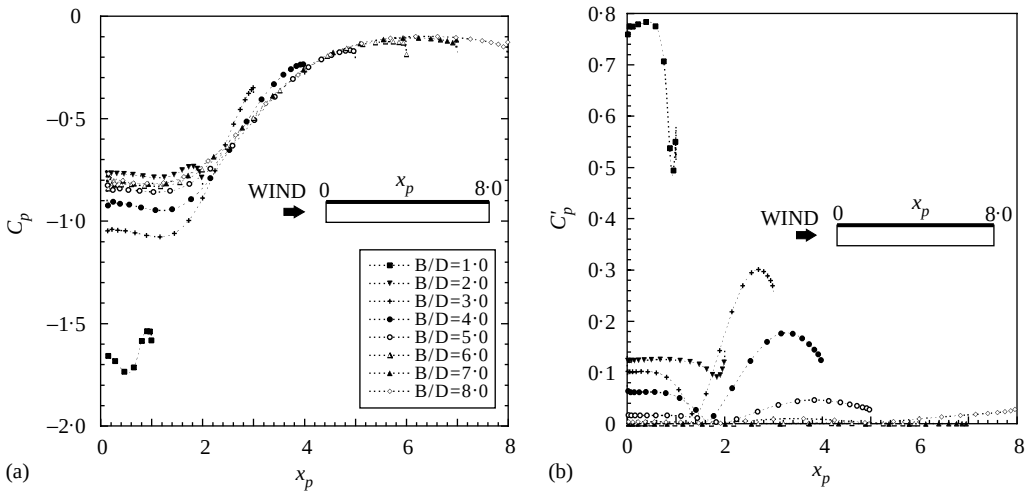

Figure 9. Pressure distribution on the side surface of various B/D ratios: (a) mean pressure coefficient; (b) fluctuating pressure coefficient.

Therefore, the time averaged characteristics are classified as those of the separated type. Also, as the side-surfaces are entirely immersed in the separated region, the fluctuating lift and pressure coefficients throughout the whole of the side-surface become large.

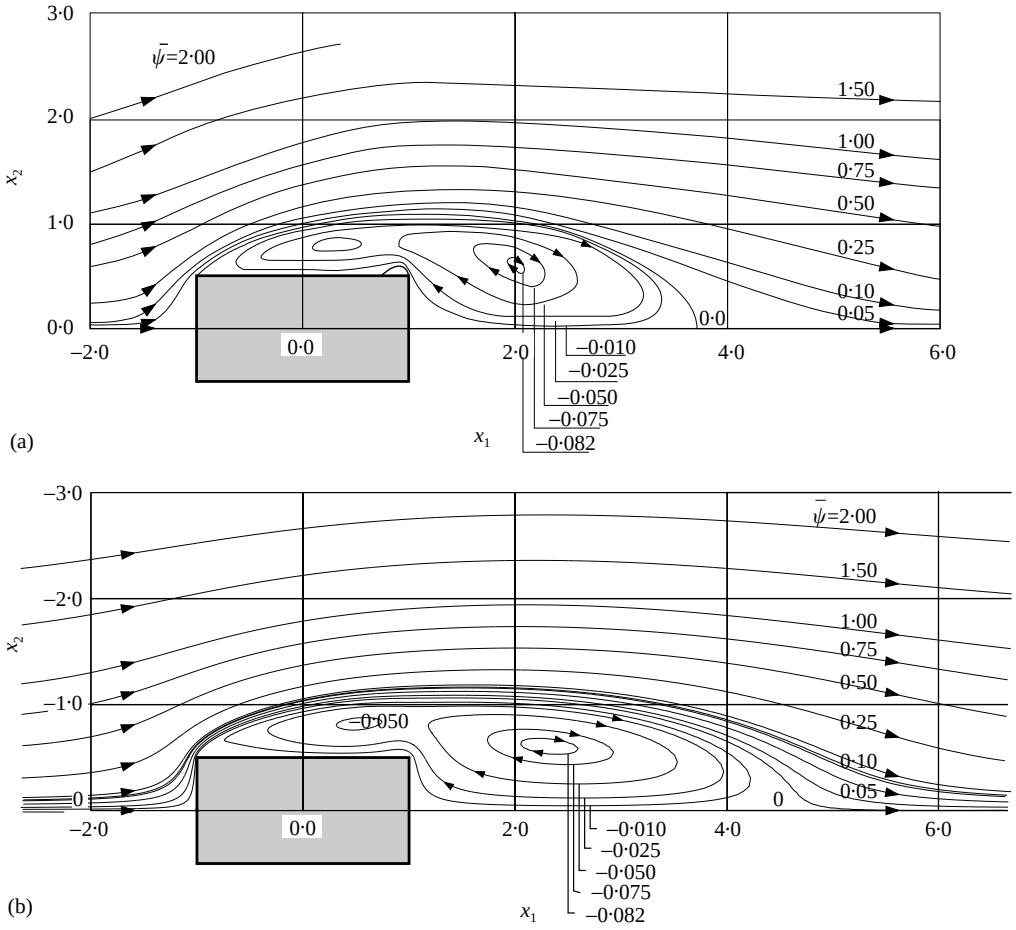

Figure 10. Comparison of time-mean streamline for $B/D = 2{\cdot}0$ rectangular cylinder: (a) measurements by Mizota & Okajima (1981), $\mathrm{Re} = 0{\cdot}714 \times 10^5$, $I = 0{\cdot}18\%$, $\gamma_b = 5\%$, $H/D = 4{\cdot}7$, where I is the turbulence intensity, γ_b the blockage ratio, and H/D the aspect ratio of the model; (b) results by the present numerical simulation.

As can be observed in Figure 7(a), the vortex behind the cross-section is closest to the cross-section for $B/D = 0{\cdot}6$ for which the mean drag coefficient is the largest. Also, it is interesting that in the wake of the cross-section the vortices are shed as a pair of streets.

As the B/D ratio increases, the location of the generation of the vortex behind the cross-section moves further away from the cylinder, up to about $B/D = 2{\cdot}0$, and coincidentally the Strouhal number becomes smaller. Almost at $B/D = 2{\cdot}0$, the generation of the vortex behind the cross-section becomes the weakest compared with other cross-sections. Also, as can be seen in Figure 8(a), the distances between the shed vortices are large, and therefore the Strouhal number is small when compared with other cross-sections.

Figure 10 shows a comparison of the time-mean streamlines for $B/D = 2{\cdot}0$ as evaluated by the present numerical simulation and from detailed measurements by Mizota and Okajima (1981) using a tandem hot-wire anemometer. They showed that at $B/D = 2{\cdot}0$ the reversed flow region is large and extends far downstream of the cross-section. Although the wake calculated by the present simulation is larger compared with that measured by them, it does correspond qualitatively with the measured wake in that the reversed flow region is extended downstream of the cross-section.

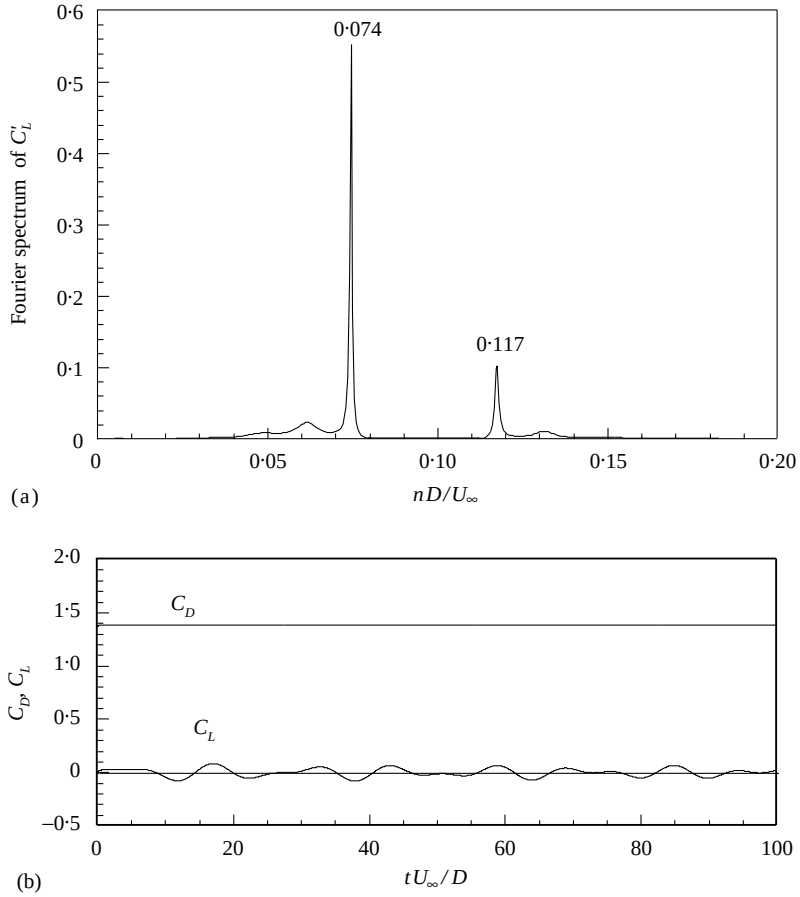

Figure 11. Fluctuation of lift on $B/D = 2{\cdot}2$ rectangular cylinder: (a) Fourier spectrum; (b) calculated time series.

Rectangular cross-sections with B/D ratios between 2·0 and 2·8 are investigated at a Reynolds number of almost 10^4 to elucidate the bimodal vortex shedding which is accompanied by an occasional reattachment of the separated shear layer onto the rearmost surfaces of the cross-sections (Okajima *et al.* 1994). In order to investigate the applicability of our numerical approach to this sensitive region where the flow reattachment on the surface occurs occasionally, calculations were made with $B/D = 2{\cdot}2$, 2·5 and 2·7. In Figure 11(a), the Fourier spectrum of the fluctuating lift as evaluated by the present approach shows double peaks at $nD/U_\infty = 0{\cdot}074$ and 0·117. On a Strouhal number chart, the higher reduced frequency ($nD/U_\infty = 0{\cdot}117$) is located between the sequences of Strouhal number plots whose B/D ratio is smaller than 2·0 (St = 0·085) and the one whose B/D ratio is larger than 3·0 (St = 0·165), and this behaviour agrees well with measurements. Although the bimodal vortex shedding is observed at $B/D = 2{\cdot}7$, the lower reduced frequency component is absent. Okajima *et al.* (1994) have also made a measurement in this region by employing hot-wire anemometry. They demonstrated that at $B/D = 2{\cdot}5$ both peaks have almost the same magnitude; however, at $B/D = 2{\cdot}8$ the higher reduced frequency mode is predominant. In general, the results of the present numerical simulation accord well with the measurement.

These bimodal frequency characteristics have been observed intermittently from measurements of the wake. That is, within a certain time range, the lower frequency

component is predominant and at other time ranges the higher frequency is predominant. The present results which are demonstrated in Figure 11(b), do not show this kind of alternating behaviour, rather the two frequency components appear as if they are combined together. This is the case because both appear as statistically equivalent, as a consequence of the ensemble averaging of the RANS model.

3.2.2. *Intermittently reattached type cross-sections* ($2{\cdot}8 < B/D < 6{\cdot}0$)

At $B/D = 3{\cdot}0$, the Strouhal number is reported to have a value between 0·16 and 0·17 in the previous experiments so that the vortex shedding period becomes small abruptly. This is well reproduced by the present numerical approach, which leads to a rapid increase in Strouhal number up to 0·167, at which time the vortex shedding immediately becomes narrower and another apparent vortex shedding appears again. Coincidentally, the fluctuating lift coefficient recovers, as seen in Figure 6(c). From a streak-line plot at $B/D = 3{\cdot}0$ in Figure 8(b), it is recognized that a separation bubble is generated on the side-surface of the cross-section. The mean pressure coefficient is lower on the windward side-surface and recovers on the leeward side, as seen in Figure 9(a). Also, the separation bubbles are alternately generated above and below the cross-section. These tendencies are observed in every cross-section almost up to $B/D = 5{\cdot}0$.

In Figure 12 is shown an example of the periodic reattachment-type cross-section for which a comparison of the time-mean streamline is made between the results of the present numerical simulation and measurements conducted by Mizota & Okajima (1981). The results of our simulation correspond well with the measured data, regarding the size of the separation bubble and that of the reversed flow region which is formed in the wake of the cylinder.

3.2.3. *Fully reattached type cross-sections* ($6{\cdot}0 \leqq B/D$)

In Figure 6(b), another discontinuity in Strouhal number can be recognized at $B/D = 6{\cdot}0$. By the way, in the vorticity contour at $B/D = 6{\cdot}0$ [Figure 7(i)] evaluated by the present numerical simulation, although a weak motion of flow can be recognized in the wake far away from the section, flow near and around the cross-section is almost close to being symmetric and thus its vortex shedding is apparently weak compared to that of other cross-sections. For neighbouring B/D ratios of 5·0 and 8·0, vortex shedding is apparently recognized. As for $B/D = 6{\cdot}0$, Nagao & Utsunomiya (1988) made experimental measurements of the flow near the side-surface by means of hot-wire anemometry and showed that there are not any apparent peaks in its spectrum. On the other hand, Tamura & Ito (1996) investigated in detail the characteristics of its fluctuating lift by using a 3-D analysis and showed the spectrum of the lift has a rather broad-band distribution and no remarkable peaks which are due to vortex shedding are recognized. The reason why in the present numerical result there is no vortex shedding and the flow is almost symmetric is because the vortex shedding is inherently weak, as is evident from comparisons of results of previous research. Although the present numerical simulation is 2-D, the presence of a region where vortex shedding is confined in the transient process from a periodical reattachment to a steady reattachment state is clarified well. This confined vortex shedding region can be found between $B/D = 6{\cdot}0$ and 7·0, as recognized from the flow pattern.

At $B/D = 8{\cdot}0$, vortex shedding resumes from the trailing edge of the section, as can be seen in Figure 7(k), and thus the Strouhal number increases again. From the streak-line plot in Figure 8(c), separation bubbles are apparent on both of the surfaces of the cross-section, and it is recognized that the flow separated from the leading edge always reattaches on both surfaces.

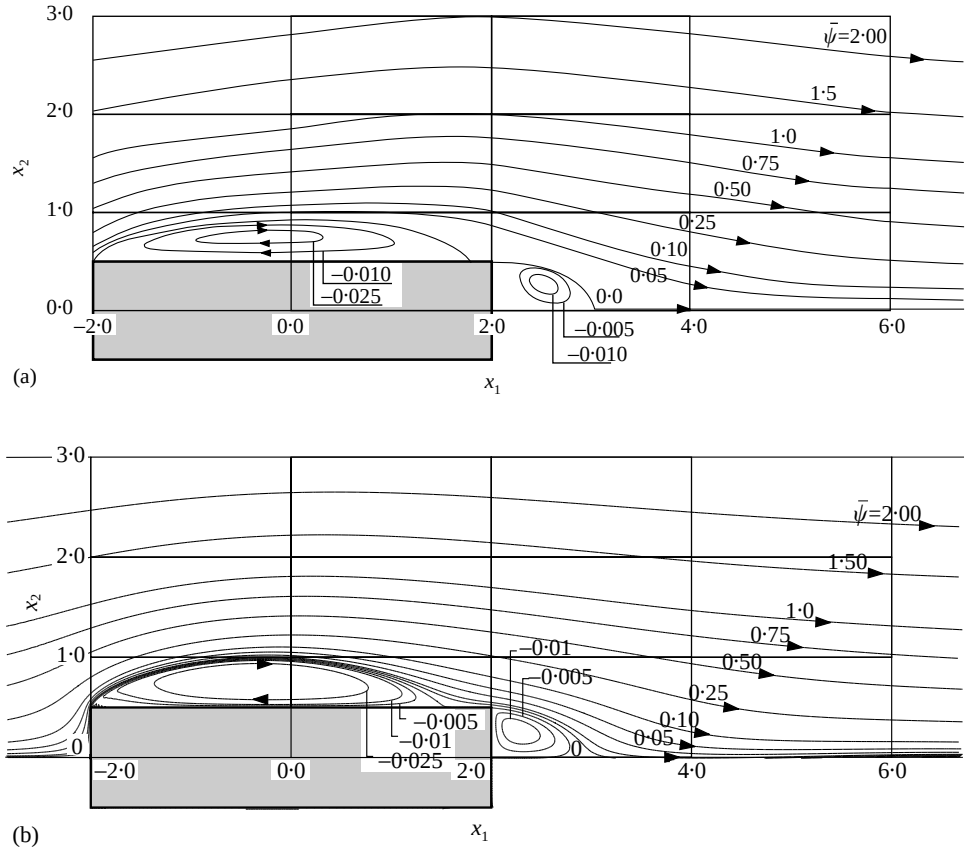

Figure 12. Comparison of time-mean streamlines for $B/D = 4{\cdot}0$ rectangular cylinder: (a) measurements by Mizota & Okajima (1981), $\mathrm{Re} = 0{\cdot}428 \times 10^5$, $I = 0{\cdot}18\%$, $\gamma_b = 3\%$, $H/D = 7{\cdot}8$, where I_{TS} the turbulence intensity, r_b the blockage ratio, and H/D the aspect ratio of the model; (b) results by the present numerical simulation.

Mean pressure coefficients of the reattachment-type cross-sections with $3{\cdot}0 \leqq B/D \leqq 8{\cdot}0$ evaluated using the present numerical simulation show that the position of the suction peak and location of the pressure recovery are almost the same. In particular, over the range $5{\cdot}0 \leqq B/D \leqq 8{\cdot}0$, the distributions are almost identical and can be expressed by one distribution along the surface. This tendency corresponds well with the results of 3-D calculations. For reattached-type cross-sections, the fluctuating pressure coefficient becomes large at the windward and leeward portions on the side-surface. When these positions are compared with the distribution of mean pressure coefficient, the large fluctuation part is seen to correspond with both the windward high-suction portion and the leeward pressure recovery portion.

3.3. Fluctuating Pressure Coefficient and Fluctuating Lift Coefficient

In the ensemble averaged model, in the case of flows with periodic unsteadiness, the instantaneous value of the physical quantity ϕ can be separated as follows (Reynolds & Hussain 1972; Franke & Rodi 1991):

$$\phi(t) = \bar{\phi} + \phi' = \bar{\phi} + \tilde{\phi} + \phi'', \tag{9}$$

where $\bar{\phi}$ is the time-mean value, ϕ' is the deviation from time-mean value, $\tilde{\phi}$ is the periodic fluctuation, and ϕ'' is the stochastic turbulent fluctuation which is uncorrelated with the periodic fluctuation. In the calculation of unsteady RANS model, the ensemble averaged value, $\bar{\phi} + \tilde{\phi}$, is directly solved from the simulation. However, the stochastic component ϕ'' is evaluated as its variance independently. Thus the variance of the total fluctuation is

$$\sigma_{\phi'}^2 = \sigma_{\tilde{\phi}}^2 + \sigma_{\phi''}^2. \tag{10}$$

For example in the unsteady calculation with the k–ε model, the variance of the periodic component of velocity is evaluated as

$$\sigma_{\tilde{u}_i}^2 = \frac{1}{T}\int_0^T \tilde{u}_i^2(t)\,\mathrm{d}t. \tag{11}$$

The stochastic component of velocity is evaluated as its variance, and is related to the turbulent kinetic energy k which is solved from its transport equation as follows:

$$\sigma_{u_i''}^2 = -\nu_t\left(\frac{\partial U_i}{\partial x_j} + \frac{\partial U_j}{\partial x_i}\right) + \frac{2}{3}k\delta_{ij} \quad (i, j = 1, 2). \tag{12}$$

However, the stochastic component of the pressure, p'', is not modelled explicitly in any current RANS models. Therefore, its total fluctuation consists of the fluctuation only by $\tilde{p}$,

$$\sigma_{p'\mathrm{RANS}}^2 = \sigma_{\tilde{p}}^2 < \sigma_{p'\mathrm{exact}}^2. \tag{13}$$

Thus, its value is always underestimated compared to the exact value of its fluctuation. Since the lift force is an integrated value of the surface pressure, the same argument holds in the prediction of the lift fluctuation. However, the extent of the underestimation is dependent on the flow regime and this can be summarized as follows.

Since the separated type cross-sections produce an apparent Karman vortex shedding and exhibit almost no reattachment, pressure fluctuations on their side-surfaces and rear-surfaces are strongly influenced by the periodic vortex shedding. For example, for the $B/D = 1{\cdot}0$ cross-section, as discussed in Section 3.1, although the present numerical simulation takes into account only the periodic fluctuation, it agrees well with the experimental and 3-D numerical results in which all components are included, as can be seen in Figure 5(b). This is because in this cross-section, the periodic component in the pressure fluctuations which is produced by cross-stream flapping of the separated shear layer is larger compared with the stochastic component. However, this flapping of the separated shear layer becomes weaker as the B/D ratio becomes slightly larger, i.e., $1{\cdot}0 < B/D < 2{\cdot}8$. This is because in these cross-sections, a weak reattachment occurs at the leeward portion of the side-surfaces and the location at which the Karman vortex is generated gradually moves away from the cross-section. Therefore, as the cross-stream flapping of the separated shear layer becomes weak and the relative contribution of the periodic component to the total fluctuation becomes small, the fluctuating lift coefficient obtained by the present numerical simulation becomes smaller than the experimental results, as exhibited in Figure 6(c). When the B/D ratio becomes still larger and apparent reattachment of the separated shear layer occurs, the relative contribution of the stochastic component to the total fluctuation becomes large. Therefore, for these "reattached type" cross-sections, quantitative differences between the simulation and experiment become noticeable. However, as there has been no research on the characteristics of the fluctuation in the aerodynamic pressures and forces by dividing them into periodic and stochastic components, it is difficult here to judge the validity of these arguments, and further studies are necessary.

4. CONCLUSION

The aerodynamic characteristics of rectangular cross-sections having infinite spanwise length with various breadth/depth ratios ranging from $B/D = 0{\cdot}6$ to $8{\cdot}0$ were investigated numerically using a two-layer k–ε model with modification on the k-production term, and its applicability to the prediction of aerodynamic characteristics of the rectangular cross-sections was examined. Results are summarized as follows:

(i) Although the present numerical approach is 2-D, it yielded physically reasonable and smooth periodic vortex shedding, even in the range of high Reynolds numbers, which cannot be simulated by ordinary 2-D analyses which do not incorporate a turbulence model.
(ii) Various typical aerodynamic features were successfully obtained, particularly including discontinuities in Strouhal number at the critical sections of $B/D = 2{\cdot}8$ and $6{\cdot}0$. Also, for various B/D ratios, the drag coefficients and the mean surface-pressure distributions were in good agreement with those from experiments and 3-D analyses.
(iii) The prediction of fluctuations in pressure and forces was considerably underestimated in some cases compared with results of experiments and 3-D analysis because of the inability of the RANS model to assess the stochastic component. The present RANS model accounts only for the periodic component.
(iv) The mean pressure distribution, particularly in the reattached-type cross-sections was well reproduced and corresponded well with the result of 3-D calculations. The occurrence of both the high suction, which is due to the appearance of a separation bubble, and pressure recovery at the leeward portion on the side-surfaces was predicted well by the present simulation.

In this paper, the aerodynamic characteristics of stationary rectangular cross-sections were discussed and it would be logical to next test its applicability to aeroelastic problems. In general, the aeroelasticity of the rectangular section is closely related to vortex shedding. Since the present simulation is able to reproduce well the intrinsic nature of instability in the vortex shedding, further applicability of the model is encouraged to extend its application to aeroelastic problems (Shimada & Meng 1998).

REFERENCES

BEARMAN, P. W. & OBASAJU, E. D. 1982 An experimental study of pressure fluctuations on fixed and oscillating square-section cylinders. *Journal of Fluid Mechanics* **119,** 297–321.

DENG, G. B., PIQUET, J. & VISONNEAU, M. 1994 2-D computations of unsteady flow past a square cylinder with the Baldwin–Lomax model. *Journal of Fluids and Structures* **8,** 663–680.

FRANKE, R. & RODI, W. 1991 Calculation of vortex shedding past a square cylinder with various turbulence models. *Eighth Symposium on Turbulent Shear Flows*, Paper 20-1, Technical University of Munich, Germany.

HARLOW, F. H. & WELCH, J. E. 1965 Numerical calculation of time-dependent viscous incompressible flow of fluid with free surface. *Physics of Fluids* **8,** 2182–2189.

KATO, M. 1997 2-D turbulent flow analysis with modified k–ε around a stationary square cylinders and vibrating one in the along and across wind direction. *Journal of Structural Mechanics and Earthquake Engineering* **I-41,** No. 577, 217–230.

KATO, M. & LAUNDER, B. E. 1993 The modeling of turbulent flow around stationary and vibrating square cylinders. *Ninth Symposium on Turbulent Shear Flows*, Paper 10-4, Kyoto, Japan.

KAWAMURA, T. & KUWAHARA, K. 1984 Computation of high Reynolds number flow around circular cylinder with surface roughness. AIAA Paper 84-0340.

LEE, B. E. 1975 The effect of turbulence on the surface pressure field of a square prism. *Journal of Fluid Mechanics* **69,** 263–282.

LEE, S. 1997 Unsteady aerodynamic force prediction on a square cylinder using k–ε turbulence models. *Journal of Wind Engineering and Industrial Aerodynamics* **67/68,** 79–90.

LYN, D. A. 1992 European research community on flow, turbulence and combustion database Case 43. http://ercoftac.mech.surrey.ac.uk/homepage.html.

MIZOTA, T. & OKAJIMA, A. 1981 Experimental studies of unsteady flows around rectangular prisms. *Proceedings of the Japan Society of Civil Engineers* **312,** 49–57.

MOCHIDA, A., MURAKAMI, S., TOMINAGA, Y. & KOBAYASHI, H. 1996 Large eddy simulation of turbulent vortex shedding flow past 2-D square cylinder using Dynamic SGS model (Part 1). *Journal of Architecture Planning and Environmental Engineering* (*Transactions of Architectural Institute of Japan*) No. 479, 41–47.

MURAKAMI, S. & MOCHIDA, A. 1995 On turbulent vortex shedding flow past 2-D square cylinder predicted by CFD. *Journal of Wind Engineering and Industrial Aerodynamics* **54/55,** 191–211.

MURAKAMI, S., MOCHIDA, A. & HAYASHI, Y. 1990 Examining the k–ε model by means of a wind tunnel test and large-eddy simulation of the turbulence structure around a cube. *Journal of Wind Engineering and Industrial Aerodynamics* **35,** 87–100.

NAGAO, F. & UTSUNOMIYA, H. 1988 The validity of sectional models on wind tunnel tests for vortex induced oscillation of bridges. *Journal of Wind Engineering and Industrial Aerodynamics* **29,** 351–360.

NAKAGUCHI, H., HASHIMOTO, K. & MUTO, S. 1968 An experimental study on aerodynamic drag of rectangular cylinders. *Journal of the Japan Society of Aeronautical and Space Sciences* **16,** 1–5.

NORRIS, L. H. & REYNOLDS, W. C. 1975 Turbulent channel flow with moving wavy boundary. Report No. FM-10, Stanford University, Department of Mechanical Engineering, U.S.A.

NOZAWA, K. & TAMURA, T. 1998 An appropriate approach to the application of large-eddy simulation to complex turbulent flow past a square cylinder. *Journal of Structural Mechanics and Earthquake Engineering* **I-43,** No. 591, 151–161.

NOZU, T. & TAMURA, T. 1997 Application of computational fluid technique with high accuracy and conservation property to the wind resistant problems of buildings and structures. *Journal of Structural and Construction Engineering* (*Transactions of Architectural Institute of Japan*), No. 494, 43–49.

OHYA, Y., NAKAMURA, Y., OZONO, S., TSURUTA, H. & NAKAYAMA, R. 1992 A numerical study of vortex shedding from flat plates with square leading trailing edges. *Journal of Fluid Mechanics* **236,** 445–460.

OKAJIMA, A. 1983 Flow around a rectangular cylinder with a section of various width/height ratios. *Journal of Wind Engineering* **17,** 1–19.

OKAJIMA, A. & SAKAI, H. 1991 Numerical simulation of flows around rectangular bodies using direct method and k–ε model. *Journal of Wind Engineering* **47,** 79–80.

OKAJIMA, A., UENO, H., YI, D. & NAKAMURA, T. 1994 Effects of Reynolds numbers on flows around a rectangular prism with side ratios of 2 to 3. *Proceedings of* 13*th National Symposium on Wind Engineering*, pp. 113–118.

OTSUKI, Y., FUJI, K., WASHIZU, K. & OHYA, A. 1978 Wind tunnel experiments on aerodynamic forces and pressure distributions of rectangular cylinders in a uniform flow. *Proceedings of the Fifth Symposium on Wind Effects on Structures*, pp. 169–176.

POCHA, J. J. 1971 On unsteady flow past cylinders of square cross-section. Ph.D. Thesis, Department of Aeronautics, Queen Mary College, London, U.K.

REYNOLDS, W. C. & HUSSAIN, A. K. M. F. 1972 The mechanics of an organized wave in turbulent shear flow. Part 3. Theoretical models and comparisons with experiments. *Journal of Fluid Mechanics* **54,** 263–288.

RODI, W. 1991 Experience with two-layer models combining the k–ε model with a one-equation model near the wall. AIAA Paper 91-0216.

SAKAMOTO, H., HANIU, H. & KOBAYASHI, Y. 1989 Fluctuating force acting on rectangular cylinders in uniform flow (on rectangular cylinders with fully separated flow). *Transactions of the Japan Society of Mechanical Engineers*, *Series B* **55,** No. 516, 2310–2317.

SHIMADA, K. & MENG, Y. 1997 Two-dimensional numerical analysis for a circular cylinder in the uniform flow by the k–ε model. *Summaries of Technological papers of Annual Meeting Architectural Institute of Japan* **B-1,** 327–328.

SHIMADA, K. & MENG, Y. 1998*a* Numerical analysis for the aerodynamic statistics of rectangular cylinders and aeroelastic vibration of $B/D = 2$ rectangular cylinder by k–ε model. *Proceedings of* 15*th National Symposium on Wind Engineering*, pp. 161–166.

TAMURA, T. & ITO, Y. 1996 Aerodynamic characteristics and flow structures around a rectangular cylinder with a section of various depth/breadth ratios. *Journal of Structural and Construction Engineering* (*Transactions of Architectural Institute of Japan*) No. 486, 153–162.

WILKINSON, R. H. 1974 On the vortex-induced loading on long bluff cylinders. Ph.D. Thesis, Faculty of Engineering, University of Bristol, England.

WASHIZU, K., OHYA, A., OTSUKI, Y. & FUJI, K. 1978 Aeroelastic instability of rectangular cylinders in a heaving mode. *Journal of Sound and Vibration* **59,** 195–210.